Dynamic Modeling and Control of Motoring-gear for Automated Guided Vehicle Powertrain Application

Yu-Chin Hsu[1)] Mi-Ching Tsai[1)*] Jia-Sheng Hu[2)] Liang-Yi Hsu[1)]
Chin-Yang Chang[1)] Chi-Yang Chang[1)] Chinweze U. Ubadigha[1)]

1) National Cheng Kung University, Electrical Motor Technology Research Center, Tainan, Taiwan
E-mail: yuchin.bill.hsu@hotmail.com; mctsai@mail.ncku.edu.tw; n1690177@nckualumni.org.tw; w0322w@gmail.com; chang.chiyang0915@gmail.com; chinwezeubadigha@gmail.com

2) National University of Tainan, Department of Greenergy, Tainan, Taiwan
E-mail: jogson@ieee.org

ABSTRACT: Electric vehicles utilizing passive drivetrains consisting of a single motor, a variable speed gearbox and differentials to provide adjustable performance capabilities are inherently riddled with mechanical complexities, poor efficiency and poor driving performance. This study investigates an alternative power transmission design for electric vehicles which is based on dual motoring-gear with special features of power split through torque and speed coupling capability. The proposed power split drivetrain consists of one main driving motor and two motoring-gear for steering control. The coaxial feature makes the drivetrain structure much simpler, and can be used as model frame for various electric vehicles and automated guided vehicles. The motoring-gear have two air gaps, and thus provide non-contact power transmission as well as torque fuse feature. The drivetrain system can be controlled to achieve both the continuously variable transmission and differential functions, such that operational power range is extended and overall performance improved. A block diagram approach is employed for analyzing the motoring-gear kinematic and dynamic characteristics, the results show that the acclaimed continuously variable transmission and differential capabilities of the proposed drive train were achieved in that steady operation is maintained under varying load conditions.

KEY WORDS: motoring-gear, drivetrain, mother frame, torque fuse.

1. INTRODUCTION

In recent years, the rise of environmental awareness has led to rapid development in technologies that utilize electric motors, drivers, and batteries. With the increasing pressure to reduce reliance on fossil fuel based vehicles, most countries around the world have been spurred to invest in the development of low-pollution, high-efficiency electric vehicles (EV). Such vehicles have been proposed as an alternative to traditional internal combustion engine vehicles that can reduce transportation costs and pollution. As a result, research related to EV drivetrains has gained much interest in recent time. Various topologies and configurations of electric motor drivetrains have been proposed to meet different design goals. Jneid et al.[(1)] described different configurations which are loosely classified based on their layouts as centralized-driven systems (Fig. 1) and, decentralized-driven systems (Fig. 2).

Centralized-driven systems consist of those drivetrains with just one motor as the main drive and connected to a mechanical gearbox and differential[(2)]. Conversely, decentralized-driven system refers mainly to those drivetrains that have more than one motor available to drive the vehicle. The main drive motor for this configuration can be located inside the wheel hub, referred to as in-wheel drivetrain[(3)~(6)], or outside of the wheel hub[(1)(6)]; and may or may not be connected to mechanical reducers or differentials.

The focus of this study will be mainly on the decentralized drivetrain located outside the wheel. Du et al.[(7)] proposed the multi-mode coupling, the speed mode coupling and the torque mode coupling drivetrains for the purpose of improving the economy of EVs. This configuration utilizes cultches, brakes and planetary gear set in coupling the dual motor and achieving the desired driving modes. Although improved efficiency can be achieved for the three different configurations when compared with the centralized-driven system, the underlying control strategy can be challenging. Zhang et al.[(8)] in their paper, proposed the use of predictive power management scheme to further improve the control and efficiency performance of the dual motor coupled with

a planetary gear set configuration. Moreover, a different drivetrain configuration which includes electronic differential (e-Differential), is proposed by Zhai et al.[9] In this configuration, three motors were utilized in total, two were used as propulsion motor and located at the left and right wheel, and one is used for steering. The propulsion motors and steering motor were coupled using two planetary gear couplers in the left and right wheel respectively. The planetary gear coupler consists of two electromagnetic clutches, two spur gear pair and a planetary gear unit. This configuration provided sufficient torque demand for different steering radius while maintaining improved steering performance. However, the configuration still made use of actuators which are drawbacks to the structural integrity and efficiency of the drivetrain. It is observed from the literature[10] that most configurations achieve mode shifting by the use of clutches, brakes or actuators. Also, only few literatures have integrated E-Differential to the drivetrain.

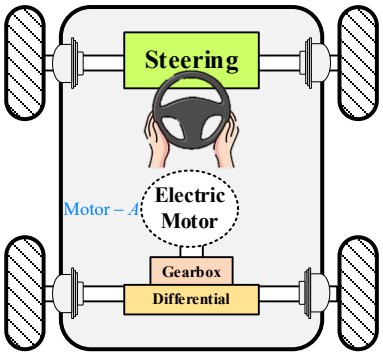

Fig. 1 Centralized electric vehicle drivetrain

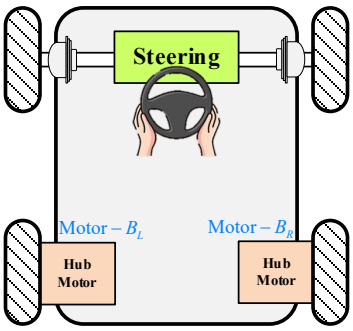

Fig. 2 Decentralized vehicle drivetrain with in-wheel drivetrain

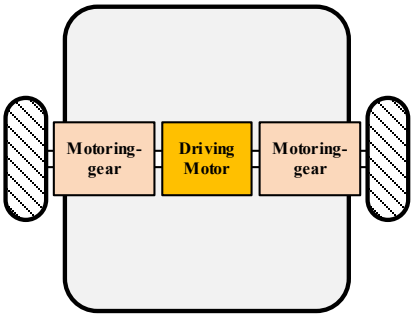

Fig. 3 Drivetrain with dual motoring-gears

This study however, proposes a drivetrain configuration that provides torque and speed control using a simple control scheme, incorporates e-Differential to the drivetrain to improve the cornering dynamics, and also achieve improved efficiency map. Fig. 3 shows the descriptive diagram of the proposed drivetrain consisting of the one driving motor and two motoring-gears located respectively on the left and right wheel base of the automated guided vehicle (AGV). Motoring-gear also known as Double Rotor Magnetic Gear Motor (DR-MGM), can work as a normal magnetic gear, and also can use stator winding to achieve the electrically continuously variable transmission (e-CVT) function. The motoring-gear structure is shown as Fig. 4, it has two mechanical ports, which are permanent magnet (PM) rotor and the modulator constructed using ferromagnetic pole pieces. The excitation of stator winding provides a rotating magnetic field that produce the required electromagnetic torque.

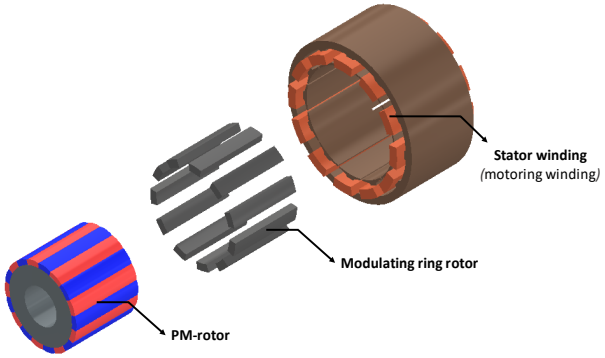

Fig. 4 Motoring-gear structure

The driving motor's output axle is connected to the PM rotor of the motoring-gears, and the modulators as output are connected to the right and left wheels respectively. The motoring-gears were adopted to effectively couple the power sources from the driving motor due to their power coupling capability. As shown in Fig. 5, the use of the motoring-gear provided one more degree of freedom, so that torque control can be implemented using the driving motor and speed control can be implemented using the stator excitation to realize the e-CVT capability.

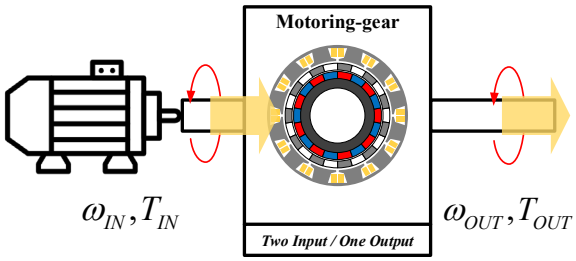

Fig. 5 Structure of the e-CVT module

2. THE MOTORING-GEAR MODEL

2.1. Motoring-gear description

Based on the DR-MGM concept, motoring-gear is a "Fully Magnetic" power module featuring magnetic actuation and magnetic transmission devices that allow for non-contact continuously variable speed transmission, and active power output. The speed ratio can be changed online via altering the frequency and amplitude of the excitations to the windings. The stator windings in the magnetic-gear motor of the motoring-gear can be controlled according to application need. By exciting the stator winding with a direct current (i.e., no rotating electromagnetic flux), the motoring-gear becomes a fixed speed ratio transmission, as with traditional gears. On the other hand, the stator driving frequency can be varied such that a variable gear ratio is achieved, thus providing active control over the stator winding and e-CVT function. Moreover, torque safety at the load end can be achieved simultaneously. Conventional motors rely on external mechanical reduction gears to increase their output torque. Motoring-gear integrates PM motor and magnetic gear transmission effectively through the careful design of drive and control architecture. By obtaining the speed and torque information, the speed control and torque safety at the load end can be simultaneously achieved via the control of the motor winding excitation.

The motoring-gear can also be found applicable as a torque fuse. Torque fuses are devices that provide machinery with torque overload protection, thus reducing damage to machinery and chance of injury to machine operators. The magnetic actuation principle of the motoring-gear allows for this feature, since a torque higher than the admissible torque of the transmission will merely cause magnetic pole slippage, as opposed to sudden failure as with traditional mechanical gears.

2.2. Motoring-Gear operating principles

Unlike the conventional passive gear transmission unit, motoring-gear is designed to perform environmental sensing functions capable of self-adjustment based on calculation and analysis according to the external mechanical power source. It can achieve dedicated, continuous, and precise output control with expanded speed/torque operational range with improved power saving. This technology has successfully established a new milestone in the electric machine drive field via software and hardware innovations. According to Fig. 4, motoring-gear is composed of a mechanical input port, stator winding control input port, and a mechanical output port. The frequency and magnitude of the magnetic field generated by the stator winding current can be controlled. The input mechanical-port is connected to the external mechanical source via the PM rotor of the motoring-gear, while the output mechanical-port is assessed via the modulator. The architecture of the DR-MGM allows for two air-gaps between the modulator, PM rotor and the stator winding to prevent them from contacting each other. The mechanical power transmission from the input mechanical-port to the output mechanical-port is delivered via magnetic field coupling. Therefore, issues such as meshing wear, pitting, and mechanical fatigue predominant in mechanical gears are avoided, without the need for lubrication and frequent maintenance.

Theoretically, the speed kinematic relation of the motoring-gear is as shown in Eq. (1), where n_{PM} is the number of pole pairs of magnets on the PM rotor, p_e is the number of pole pairs of the stator winding, and q_{mod} is the number of iron pole pieces of the modulator. It is noted that number of iron pole pieces of the modulator must be the sum of pole pairs of PM rotor and stator winding ($q_{mod} = p_e + n_{PM}$). Also, the electrical magnetic rotational speed of winding excitation, modulator and PM rotor are denoted by ω_e, ω_{mod} and ω_{PM} respectively.

$$\omega_{Mod} = \frac{n_{PM}}{q_{Mod}}\omega_{PM} + \frac{p_e}{q_{Mod}}\omega_e \quad (1)$$

Where the rotational speed of the magnetic field ω_e generated by AC electrical power can be expressed in rpm (revolution per minute) as:

$$\omega_e = \frac{60 * f}{p_e} \quad (2)$$

f is the coil winding excitation frequency. The motion relation of Eq. (1) indicated that when the rotational magnetic field (ω_e) of stator winding is along the same direction as the input rotational speed of the PM rotor (ω_{PM}), motoring-gear mechanical output rotor accelerates; on the contrary, when the direction of the rotational magnetic field is in the opposite direction to the rotational speed of the PM rotor, the motoring-gear mechanical output decelerates.

This acceleration and deceleration feature gives the motoring-gear a wider and more flexible speed-controlled range. Also, the motoring-gear is equipped with continuously variable speed transmission function which is made possible by controlling the magnetic field of the stator winding with respect to the PM rotor speed. For the special case of the coil winding being DC excited (i.e., $\omega_e = 0$), the transmission between the PM rotor and the modulator has a fixed gear ratio. In other words, the use of motoring-gear grants the system higher degree of freedom. Instead of being limited to the combinations of gear pairs with specific speed ratios, different speed ratios and torque ratios can be readily

and timely switched by applying appropriate smart control scheme that meets the requirements of the desired application.

3. E-CVT AND E-DIFFERENTIAL STRATEGY

The major function of the motoring-gear in this paper is to achieve the e-CVT on an AGV. To specify the variable speed ratio and the differential function, block diagram method is used to describe the drivetrain structure and the control strategy.[11]~[13]

3.1 Proposed dual e-CVT structure

This paper proposes a drivetrain module based on dual motoring-gears, which aims to achieve the electronically controlled CVT (e-CVT), also proposed electronically controlled differential steering system (e-DSS). As Fig. 6 shows, the dual motoring-gears drivetrain module are used to control the left and the right wheels of the AGV. In addition to two motoring-gears, a driving motor is linked to the PM rotors in both of the motoring-gears, and the stator winding assists to vary the speed ratio of the e-CVT configuration. Based on the kinematic characteristic of motoring-gear, with the driving motor's power input and the stator excitation, the modulator output speed can be dynamically controlled. To achieve e-CVT function, the transmission index α is defined to obtain the angular speed ω_e of the stator excitation based on the driving motor input. According to the kinematic motion relation of motoring-gear, the output angular speed of the modulator ω_{Mod} can be obtained as shown in Eq. (3). By modifying the transmission index α, variable speed ratio can be reached to achieve the e-CVT function.

$$\omega_{Mod} = \left(\frac{n_{PM} + \alpha p_e}{q_{Mod}}\right)\omega_{PM} \tag{3}$$

As shown in the block diagram, the stator winding acts as a secondary input to the drivetrain module, the speed relationship of the proposed dual motoring-gears configuration is expressed in Eq. (4), where ω_{Mod}^L and ω_{Mod}^R denoted the output angular speeds of the left and right wheels respectively; ω_e^L and ω_e^R are the electrical angular speed of the stator winding.

$$\begin{cases} \omega_{Mod}^L = \dfrac{n_{PM}}{q_{Mod}}\omega_{PM} + \dfrac{p_e}{q_{Mod}}\omega_e^L \\ \omega_{Mod}^R = \dfrac{n_{PM}}{q_{Mod}}\omega_{PM} + \dfrac{p_e}{q_{Mod}}\omega_e^R \end{cases} \tag{4}$$

Thus, the driving motor is controlled in torque mode in order to produce sufficient torque while carrying load. The dynamic relationship between torque and the speed of the driving motor is shown as Eq. (5), where T_{Dri} is the input torque generated by the driving motor, J_{Dri} and B_{Dri} are the moment of inertia and the damping coefficients of the driving motor, respectively.

$$\omega_{Dri} = \frac{1}{J_{Dri} + B_{Dri}} T_{Dri} \tag{5}$$

As mentioned before, transmission index α is defined to achieve e-CVT function of the drivetrain module. Thus, the speed ratio between driving motor input and modulator output can be modified. Let $\alpha(\omega_{Dri}) = \omega_e^L/\omega_{Dri}$ be the e-CVT transmission index and, $f(\alpha) = \omega_e^R/\omega_{Dri}$ be the e-DSS speed regulation ratio. Also, $\alpha(\omega_{Dri})$ and $f(\alpha)$ denote the left and right wheel transmission indexes respectively. The $\alpha(\omega_{Dri})$ will be used in realizing e-CVT functionality, and is a function of the driving motor speed. Similarly, $f(\alpha, R)$ is aimed to be use in the e-DSS control which is a function of both steering radius and driving motor speed. The block diagram of a proposed steering-drive transmission control structure is shown in Fig. 7.

Fig. 6 Dual Motoring-gear Drivetrain Module

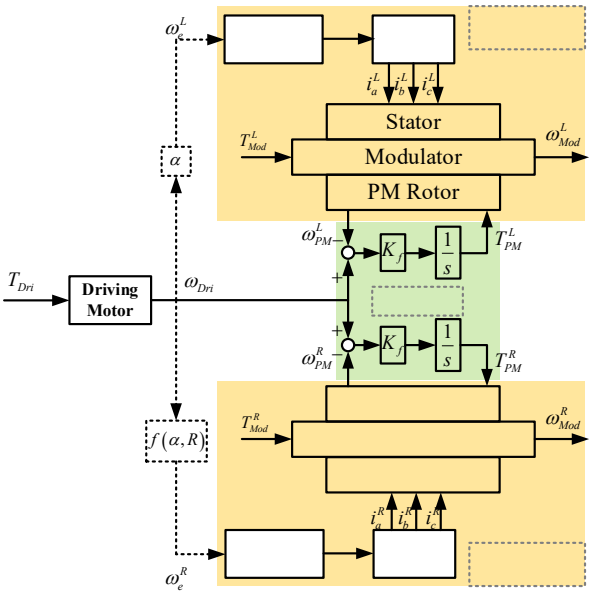

Fig. 7 Block Diagram of the differential-drive structure

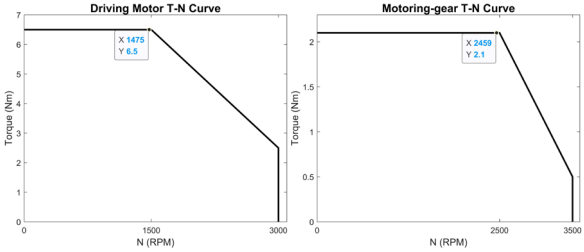

Fig. 8 T-N Curve of Driving Motor and Motoring-gear

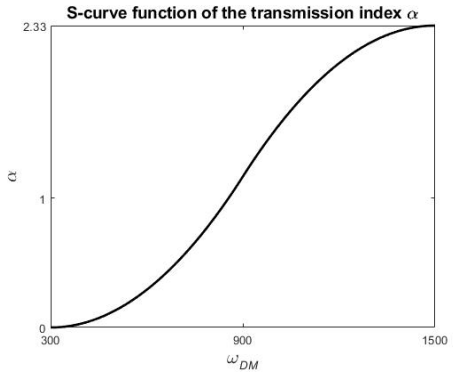

Fig. 9 S-curve of transmission index α

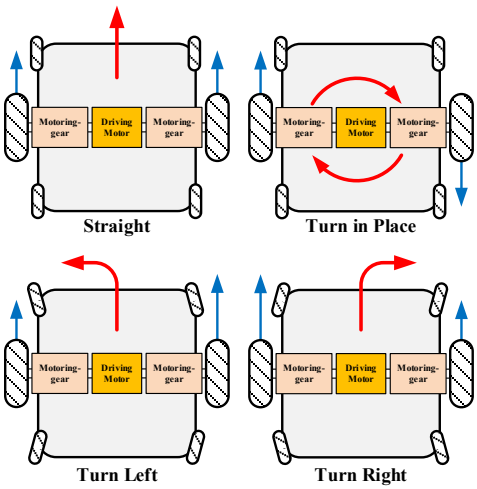

Fig. 10 Differential drive AGV steering principle

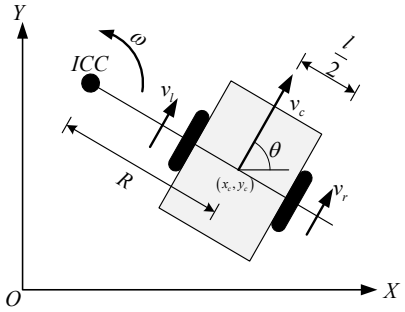

Fig. 11 2-D plane AGV motion coordinate system

3.2 Dual e-CVT regulation strategy

Based on the T-N curves of the driving motor and motoring-gears, the speed regulator strategy for the e-CVT is designed. As shown in Fig. 8, the maximum speed of the driving motor is 3000 rpm and the rated torque is 6.5 Nm@1500 rpm, the maximum speed of the motoring-gear excitation is 3500 rpm, and the rated torque is 2.1 Nm@2500 rpm. There are three different operating modes corresponding to various transmission index α. If the driving motor is operated at the rated speed, and the maximum speed of motoring-gear previously given as 3500 rpm, the maximum transmission index α will be around 2.3 as defined in Fig. 9. The specifications of the motoring-gears employed in this paper are listed in Table I. Therefore, the controlled speed ratio between driving motor input and modulator output is the resulting from 0.81 to 1.25 according to Eq. (3).

Table I Motoring-gear Parameters

Parameters	Description	Value
p_e	Pole pairs number of stator winding and PM rotor, and number of ferromagnetic	2
n_{PM}		9
q_{Mod}		11

The e-CVT control strategy switch the mode under two speed thresholds, which are denoted as ω_L and ω_H. The first switching threshold, ω_L, is decided based on the rotating speed of the driving motor. The other switching threshold, ω_H, is decided according to the rated speed of the driving motor, also the motoring-gear. For the purpose of reducing the impact of mode switching on the drivetrain system, the range of the transmission index $\alpha(\omega_{Dri})$ is expressed via S-curve function as:

$$\alpha(\omega_{Dri}) = \begin{cases} 0; & \omega_{Dri} \le \omega_L \\ S(\omega_{Dri}, \omega_L, \omega_H); & \omega_L \le \omega_{Dri} \le \omega_H \\ 2.3; & \omega_{Dri} > \omega_H \end{cases} \quad (6)$$

Where the S-curve is given as Eq. (7) and illustrated in Fig. 9.

$$S(\omega_{Dri}, \omega_L, \omega_H) = \begin{cases} 4.6\left(\frac{\omega_{Dri} - \omega_L}{\omega_H - \omega_L}\right)^2; & \omega_L \le \omega_{Dri} \le \frac{(\omega_L + \omega_H)}{2} \\ 2.3 - 4.6\left(\frac{\omega_H - \omega_{Dri}}{\omega_H - \omega_L}\right)^2; & \frac{(\omega_L + \omega_H)}{2} \le \omega_{Dri} \le \omega_H \end{cases} \quad (7)$$

When the PM rotor or the driving motor speed, $\omega_{PM} = \omega_{Dri}$, is lower than the first threshold ω_L, the transmission index $\alpha(\omega_{Dri}) = 0$, which means the stator excitation is stationary. As the driving motor speed ω_{Dri} increases, within the threshold range, $\omega_L \le \omega_{Dri} \le \omega_H$, $\alpha(\omega_{Dri})$ increases according to the defined sigmoid function. The transmission index reaches a maximum of $\alpha(\omega_{Dri}) = 2.3$ when the driving motor speed exceeds the threshold value ω_H to ensure that a speed command exceeding the limit is not produced. Base on this sigmoid function and various driving scenario, the speed ratio between the driving motor and the modulator output can be actively changed. Thus, the speed commands of the two motoring-gears in Fig. 9 can be obtained as,

$$\begin{cases} \omega_e^L = \alpha(\omega_{Dri}) \cdot \omega_{Dri} \\ \omega_e^R = f(\alpha, R) \cdot \omega_{Dri} \end{cases} \quad (8)$$

where R denotes the steering radius. The speed ratio $f(\alpha, R)$ is defined for achieving the actively controlled differential steering. Therefore, Eq. (8) can be rewritten as follows:

$$\begin{cases} \omega_{Mod}^L = \left(\frac{n_{PM} + \alpha(\omega_{Dri}) p_e}{q_{mod}}\right) \omega_{Dri} \\ \omega_{Mod}^R = \left(\frac{n_{PM} + f(\alpha, R) p_e}{q_{mod}}\right) \omega_{Dri} \end{cases} \quad (9)$$

3.3 AGV Steering Principle

Differential drive structure AGV consists of two driving wheels, which are mounted on a common axis. As shown in Fig. 10, varying the wheels' speed can achieve different AGV movements, such as moving straight, making a U-turn and turning left or right. The schematics of the differential drive is shown as Fig. 11, when steering the AGV, the point of rotation lies along the common left and right wheel axis, and is known as Instantaneous Center of Curvature (*ICC*). The velocities of the two wheels v_l and v_r can be written as Eqs. (10)~(11), where ω is the rotation rate about ICC, R is the distance from the *ICC* to the midpoint of AGV, l is the track width.

$$v_l = \omega\left(R + \frac{l}{2}\right) \tag{10}$$

$$v_r = \omega\left(R - \frac{l}{2}\right) \tag{11}$$

$$v_c = \frac{v_r + v_l}{2} \tag{12}$$

At any instance in time, the AGV's rotation rate and rotation distance can be obtained as,

$$v_l = v_c\left(1 + \frac{l}{2R}\right) \tag{13}$$

$$v_r = v_c\left(1 - \frac{l}{2R}\right) \tag{14}$$

Assuming there is no slip when the AGV is operating, the movement of AGV on a 2-D plane can be controlled based on the e-Differential steering system. The steering radius command R determines the speed ratio between the left wheel and right wheel during curving. The differential ratio between left and right wheels is defined as $M(R)$, which is actively controlled according to the steering radius command R, and can be expressed as follows:

$$M(R) = \frac{v_r}{v_l} = \frac{2R - l}{2R + l} \tag{15}$$

Furthermore, the required speed $f(\alpha, R)$ in terms of synchronized ratio $M(R)$ is expressed as,

$$f(\alpha, R) = M(R)\left[\left(1 - \frac{1}{M(R)}\right)\frac{n_{PM}}{p_e} + \alpha(\omega_{Dri})\right] \tag{16}$$

The differential ratio $M(R)$ varies with respect to the steering radius command input. For the case of straight motion, $M(R) = 1$, and Eq. (16) becomes $f(\alpha, R) = \alpha$. A synchronized motion control method is then designed to realize e-CVT and e-Differential capabilities.

4. SIMULATION AND EXPERIMENTAL RESULTS

The capabilities of the dual motoring-gear drivetrain module include the e-CVT and e-DSS functions, its control strategy is verified in MATLAB Simulink using the block diagram description of Fig. 7. The parameters used for simulation are list in Table II, which is decided based on the FEM model of the motoring-gear and the specification of the driving motor. In addition, the AGV's parameters are defined by the prototype shown in Fig. 12. The simulated system of the proposed active drivetrain system includes a driving motor connected to two motoring-gears, a load is applied at the modulator to simulate the environmental load. From the simulation, the e-CVT and e-DSS control strategy effect can be observed.

4.1 Simulation Results

Fig. 13 shows the simulation results from the regulation strategy designed to verify the function of the e-CVT and e-DSS. To let the AGV startup gently, the torque command of the driving motor is increased until smooth output speed response is achieved. When the driving motor speed is lower than the first threshold, the speed ratio is zero, which provides high output torque on the wheel to move the AGV from rest. As the driving motor speed increases, the stator is excited to increase the speed ratio and achieve the e-CVT function. Once the AGV start operating at steady velocity, the steering radius is given to verify the e-DSS function. The AGV is commanded going straight within 0s to 10s; within 10s to 20s, the steering radius command R is set 3000mm along the common left and right wheels axis; within 20s to 30, the AGV is commanded going straight. As illustrated in Fig. 13(c), the differential ratio is adjusted according to the steering radius command, the e-DSS function is achieve since the left and right wheels have different output speed as shown in Fig. 13(d).

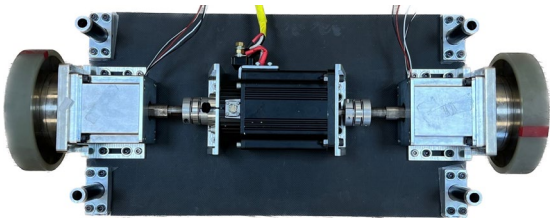

(a) Dual motoring-gear drivetrain

(b) AGV Prototype

Fig. 12 Test models

Table II Simulation Parameters

Parameters	Value	Unit
Driving motor inertia, J_{Dri}	3.837e-3	$kg \cdot m^2$
Driving motor damping coefficient, B_{Dri}	2.095e-3	$\frac{Nm \cdot s}{rad}$
Motoring-gear PM rotor inertia, J_{PM}	4.502e-3	$kg \cdot m^2$
Motoring-gear PM rotor damping coefficient, B_{PM}	2.864e-3	$\frac{Nm \cdot s}{rad}$
Motoring-gear Modulator inertia, J_{Mod}	5.502e-3	$kg \cdot m^2$
Motoring-gear Modulator damping coefficient, B_{Mod}	3.564e-3	$\frac{Nm \cdot s}{rad}$
AGV track width	800	mm
AGV wheel radius	100	mm
AGV total weight	60	kg

(a) Driving motor output speed

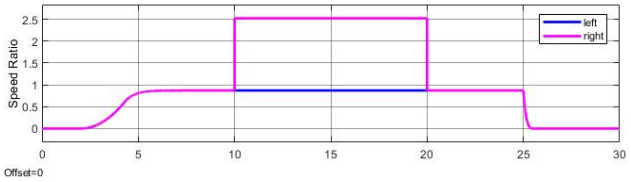

(b) Speed Ratio

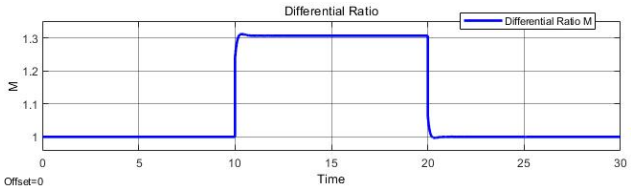

(c) Differential ratio

(d) Wheel speeds

Fig. 13 Simulation results of the regulation strategy

4.2 Experimental Results

Fig. 14 shows the experiment results from the regulation strategy designed to verify the capabilities of e-CVT and e-DSS functions with different driving scenarios. First, as illustrated in Fig. 14(a), the speed of the main driving motor increases corresponding to the torque command. As the driving motor speed increasing, Fig. 14(b) shows that the e-CVT is controlled at a low-speed ratio, so that a higher starting torque is provided for acceleration. As the AGV is brought to speed, the motoring-gears' stator is excited to increase the speed ratio so that output speed continues to increase for high-speed cruising. Finally, the differential ratio is adjusted according to the steering radius command as shown in Fig. 14(c), which displays the e-DSS function necessary for curve maneuvers during which, the left and right wheels have different output speeds as illustrated in Fig. 14(d).

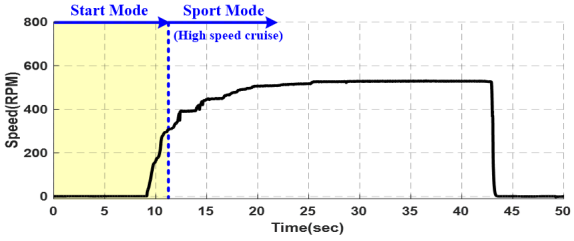

(a) Driving motor output speed

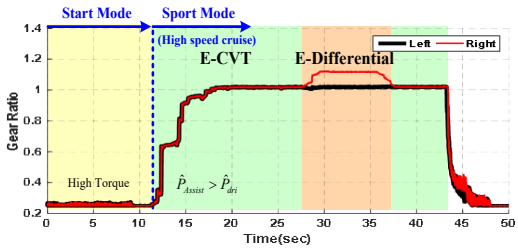

(b) Speed ratio

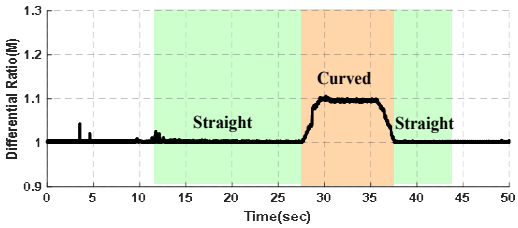

(c) Differential ratio

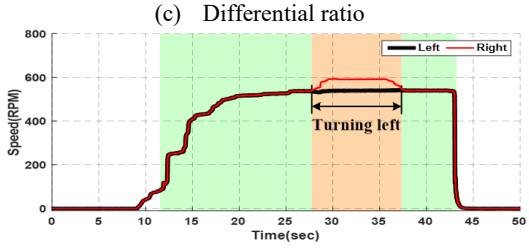

(d) Wheel speeds

Fig. 14 Experimental results of the regulation strategy

5. CONCLUSION

This study has presented a drivetrain comprising of one torque control driving motor and two motoring-gears on the left and right wheel of AGV through speed motion control for achieving e-CVT and e-DSS functions. Based on differential drive AGV system analysis, the e-CVT and e-DSS functions are implemented based on driving motor torque command and steering radius commands,

which currently are programmed on the control MCU on the prototype AGV. Different speed regulation strategy modes are employed in the control scheme in order to simulate different operating scenarios such that the system exhibits CVT and differential capabilities. According to the simulation and experiment results, the aimed functions of the dual motoring-gears drivetrain module are validated. The AGV is shown to be capable of different modes of operation as well as displaying stable straight and curved motions. In future development, this study will incorporate into the prototyped AGV a guidance system, such as SLAM system or magnetic tape guidance to generate the steering radius command automatically. Also, more robust control strategy will be applied to improve the performance of the AGV, like load torque observer, synchronized motion control to enhance the robustness of the drivetrain system.

ACKNOWLEDGMENT

This work was supported by the National Science and Technology Council (NSTC), Taiwan, under Grant 109-2622-8-006-005, 111-2222-E-024-001, and 111-2218-E-006-013.

REFERENCES

(1) M. S. Jneid, P. Harth, and P. Ficzere, “In-wheel-motor electric vehicles and their associated drivetrains”, *International Journal for Traffic and Transport Engineering 2*, vol. 10, no. 4, pp. 415-431, Oct 2020.

(2) M. Ehsani, K. M. Rahman, M. D. Bellar and A. J. Severinsky, “Evaluation of soft switching for EV and HEV motor drives,” *IEEE Transactions on Industrial Electronics*, vol. 48, no.1, pp. 82-90, Jun 2001.

(3) R. N. Tuncay, O. Ustun, M. Yilmaz, C. Gokee, and U. Karakaya, “Design and implementation of an electric drive system for in-wheel motor electric vehicle applications,” *2011 IEEE Vehicle Power and Propulsion Conference*, pp. 1-6, Chicago, IL, USA, Sept 6-9, 2011.

(4) G. Nagaya, Y. Wakao, and A. Abe, “Development of an in-wheel drive with advanced dynamic-damper mechanism”, *JSAE Review*, vol. 25, no.4, pp 477-481, Oct 2003.

(5) A. Watts, A. Vallance, A. Whitehead, C. Hilton, and A. Fraser, “The technology and economics of in-wheel motors,” *SAE International Journal of Passenger Cars - Electronic and Electrical System*, vol. 3, no. 1, pp. 37-55, Oct 2010.

(6) J. J. Eckert, L. C. Silva, E. S. Costa, F. M. Santiciolli, F. G. Dedini, and F. C. Corrêa, “Electric vehicle drivetrain optimisation,” *IET Electrical Systems in Transportation*, vol. 7, no. 1, pp. 32-40, Mar 2017.

(7) W. Du, S. Zhao, L. Jin, J. Gao, and Z. Zheng, “Optimization design and performance comparison of different drivetrains of electric vehicles,” *Mechanism and Machine Theory*, vol. 156, no. 1, pp. 104-143, Feb 2021.

(8) C. Zhang, S. Zhang, G. Han, and H. Liu, "Power Management Comparison for a Dual-Motor-Propulsion System Used in a Battery Electric Bus," *IEEE Transactions on Industrial Electronics*, vol. 64, no. 5, pp. 3873-3882, Nov 2017.

(9) L. Zhai, H. Huang, and S. Kavuma, “Investigation on a power coupling steering system for dual-motor drive tracked vehicles based on speed control,” *Energies*, vol. 10, no. 8, pp. 1118, Jun 2017.

(10) R. H. Haas and R. C. Manwaring, "Development of a limited slip differential," *SAE Transactions*, vol. 80, no. 3, pp. 2175-2193, 1971.

(11) J. Wojnarowski, “The graph method of determining the loads in complex gear trains,” *Mechanism and Machine Theory*, vol. 11, no. 2, pp. 103-121, 1976.

(12) J. Wojnarowski, and A. Lidwin, “The application of signal flow graphs—the kinematic analysis of planetary gear trains,” *Mechanism and Machine Theory*, vol. 10, no. 1, pp. 17-31, Feb, 1975.

(13) C. U. Ubadigha, and M. C. Tsai, “Analysis of Integrated Magnetic Gear Motor with Dual Mechanical Output Port: A Block Diagram Approach,” *IEEE Transactions on energy conversion*, vol. 335, no. 3, pp. 1301-1308, Sept, 2020.

(14) Y. E. Zhao and H. Zhang, “Modelling and simulation of the electronic differential system for an electric vehicle with two-motor-wheel drive,” *International Journal of Vehicle Systems Modelling and Testing*, vol. 4, no. 1-2, pp. 117-131, Jul, 2009.